Precipitation Extremes and Flood Frequency in a Changing Climate in Southeastern Virginia

Venkataramana Sridhar[1]*, Parthkumar Modi[1], Mirza Billah[2], Prasanth Valayamkunnath[1], Jonathan L. Goodall[3]

[1]Department of Biological Systems Engineering, Virginia Tech, Blacksburg, Virginia, USA

[2]South Florida Water Management District, West Palm Beach, Florida, USA

[3]Department of Civil and Environmental Engineering, University of Virginia, Charlottesville, Virginia, USA

*Correspondence to Sridhar: vsri@vt.edu

Research Impact Statement

Extreme events pose a challenge to Coastal Southeast Virginia. A 2 - 3 times increase in 24- and 48-hr precipitation intensity resulting in up to 50% increase in flood flows are likely in the future.

Abstract

Despite the advances in climate change modeling, extreme events pose a challenge to develop approaches that are relevant for urban stormwater infrastructure designs and best management practices. The study first investigates the statistical methods applied to the land-based daily precipitation series acquired from the Global Historical Climatology Network-Daily (GHCN-D). Additional analysis were carried out on the simulated Multivariate Adaptive Constructed Analogs (MACA)-based downscaled daily extreme precipitation of 15 General Circulation Models (GCMs) and Weather Research and Forecasting (WRF)-based hourly extreme precipitation of North American Regional Reanalysis (NARR) to discern the return period of 24-hr and 48-hr events. We infer that the GHCN-D and MACA-based precipitation reveal increasing trends in annual and seasonal extreme daily precipitation. Both BCC-CSM1-1-m and GFDL-ESM2M models revealed that the magnitude and frequency of extreme precipitation events are projected to increase between 2016-2099. We conclude that the future scenarios showed an increase in magnitudes of extreme precipitation up to 3 times   across southeastern Virginia resulting in increased discharge rates at selected gauge locations. The depth duration frequency curve predicted an increase of 2 to 3 times in 24- and 48-hour precipitation intensity, higher peaks and indicated an increase of up to 50% in flood magnitude in future scenarios.

Keywords: Precipitation, Extremes, IDF Analysis, Peak flows, Climate Change, Coastal Virginia

1
2
3   **INTRODUCTION**
4
5   Globally, increased frequency and magnitude of extreme precipitation events have
6
7   become a regular phenomenon in the past two decades (Karl and Knight, 1998; Osborn et al.,
8
9   2000; Sen Roy and Balling, 2004; Solomon et al., 2007; Camici et al., 2013; Maurer et al., 2018;
10
11   Mukherjee et. al., 2018). The impacts due to these changes are expected to be intensified by the
12
13   human-induced land use and climate changes (Min et al., 2011; Wuebbles et al., 2014).
14
15   The impact of extreme and frequent precipitation events over urban areas due to climate
16
17   change are more significant, as these areas are the centers of human activities (Rosenzweig et al.,
18
19   2010, Mishra et. al., 2015, Ali and Mishra, 2018). Urban centers are the focal point of climate
20
21   change adaptation due to rapidly changing conditions arising from global warming (Brown,
22
23   2001). The population in urban areas is expected to increase to 60% by 2030 and 70% by 2050
24
25   (World Health Organization, 2014). Hence, the adequacy of the built infrastructure in urban
26
27   areas is dependent on resilient designs and better understanding of extreme precipitation
28
29   characteristics. The detailed understanding of extreme precipitation characteristics is essential to
30
31   plan and manage these infrastructures in the urban environment (Mishra and Lettenmaier, 2011;
32
33   Camici et al., 2013). These infrastructure systems often fail to accommodate extreme
34
35   precipitation-generated maximum floods due to the traditional consideration of constant
36
37   statistical parameters of the hydrologic variables (Denault et al., 2002). While considering the
38
39   design parameters, the stationarity principles ignore the increases in both intensities and
40
41   magnitudes of precipitation. The application of the Depth-Duration-Frequency (DDF) approach
42
43   is a standard practice in designing hydrologic systems that incorporate magnitude, frequency,
44
45   and duration of precipitation events (Liew et al., 2014; Alam and Elshorbagy, 2015). However,
46
47   changes in the hydrologic cycle, which mainly includes precipitation, surface runoff, streamflow
48
49   and groundwater or recharge, are exclusively responsible for flooding conditions, and therefore,
50
51
52
53
54
55
56
57
58
59
60

applying the DDF approach needs to be adjusted with a high spatial and temporal analysis of observed and simulated precipitation and runoff data.

However, attempts to characterize trends in precipitation extremes are hindered by a lack of long-term and high-resolution climate and hydrological variables in urban areas. Fewer weather stations, uncertainties in measurements, and the period of record compound the problems in detecting trends as well as performing the attribution analysis (Groisman and Easterling, 1994). In addition to these challenges, several other factors complicate the robust and compelling pattern detection of extreme precipitation. The non-normal distribution, serial correlation, outliers, and missing data can influence the trend analysis of statistical significance (Khaliq et al., 2009; McAfee et. al., 2013). Thus, the cumulative role of these factors contributes to a high level of disagreement regarding the magnitude and direction of precipitation events in urban areas. Particularly, smaller catchments in the coastal region that are under a constant risk of flooding, either through high-stage streams flowing from inland or increases in mean sea level, are poorly understood due to the lack of observational points and modeling efforts.

Gridded datasets of precipitation and hydrologic variables are often developed to overcome the above shortcomings for these areas and to provide a more geographically complete weather and climate assessment. Additionally, the runoff generated from heavy precipitation events is difficult to estimate because of topographic and land surface hydrological conditions in developed areas. There are differences in both climate and hydrological model predictions and these differences propagate from the respective models, which may then contribute some level of inconsistency among the gridded datasets of climate and hydrological variables (Hofstra et al., 2009). Arriaga-Ramírez and Cavazos (2010) found increased seasonal and annual trends using monthly precipitation at spatial scales of northwest Mexico and southwest United States. Mishra

and Lettenmaier (2011) and Mishra et al. (2015) estimated the linear trends of historical

precipitation in the urban and surrounding non-urban areas of the United States. McAfee et al.

(2013, 2014) investigated the trend using both station- and grid-based precipitation from 1950-

2010 and reported temporal changes in the trends along with substantial differences among the

gridded datasets in terms of intensity and interannual variability in Alaska. Chen and Frauenfeld

(2014) applied Coupled Model Intercomparison Project Phase 5 (CMIP5) models to capture

historical precipitation trends and future predictions using Representative Concentration

Pathways (RCP) scenarios. However, the mean of the CMIP5 models was unable to capture the

magnitude for multi-decadal precipitation variability due to coarse scale precipitation estimates.

Camici et al. (2013) revealed that downscaled General Circulation Models (GCMs) and

downscaling approaches could be a factor in evaluating and predicting annual precipitation

extremes. The possibility of capturing and forecasting these trends increases with increased

involvement of downscaled GCMs (Crétat et al., 2014).

There is a critical need in understanding extreme precipitation patterns and resultant

peak runoff due to the presence of the largest naval base and other security installations in

southeastern Virginia. We performed a comprehensive evaluation of precipitation trends in

southeastern Virginia by examining the records of long-term precipitation at station locations

from the Global Historical Climatology Network-Daily (GHCN-D) and by performing a

hydrological simulation analysis in the James River basin (for streamflow measurements). Using

both station-based and model-based downscaled gridded precipitation data, we investigated the

magnitude, distribution, and direction of the extreme precipitation and streamflow characteristics

for both historical and future periods. We used historical and future design storm events to

generate flood frequency curves that reflect historical and future changes in rainfall intensity

for1950-2099. We included Multivariate Adaptive Constructed Analogs (MACA) based downscaled precipitation from GCMs of the CMIP5 products to evaluate the capability of the models and capture the historical events, to assess uncertainties in characterizing precipitation patterns and to forecast the future extreme precipitation events. We investigated the changes in streamflow using a combination of Variable Infiltration Capacity (VIC) and the Noah Multi-Physics (Noah MP) land surface models (LSMs) for different return periods. We, therefore, analyzed the changes in extreme precipitation characteristics using a suite of precipitation products and performed a flood frequency analysis by translating the extreme precipitation into runoff using the hydrology models.

METHODS

Data Construction and Characteristics

High-resolution design intensities of extreme rainfall events are imperative for assessing the impact of climate change over urban areas (Arbbjerg-Nielsen, 2012). This is due to the ability of these models to capture many hydrologic processes that occurred at finer scales and to avoid under or overestimation of the design storm for the subsequent analysis. Therefore, our selection of precipitation data and climate models was conducted with caution to comprehend important hydrologic processes in the urban region. We first selected the urban region and then focused on collecting and generating high-resolution data to compute a storm design. The extreme precipitation term was characterized based on the precipitation amount at temporal and spatial scales. For both station observation and gridded products, a daily precipitation amount was considered extreme when it exceeded the 90th percentile threshold computed for all rainy days. The rainy days were defined as the days with precipitation of at least 1 mm. The

precipitation data were analyzed by applying four different statistical tests (Linear Regression, Mann-Kendall Trend Analysis, Theil-Sen Slope Estimator, and Kolmogorov-Smirnov Test) for 1950-2099. The linear regression statistics have a limitation in providing reliable assessments of trends and distributions. However, the three other approaches are not only considered robust and consistent, but in combination they can also provide a complete understanding of the direction and distribution of extreme precipitation events.

Study Area

Figure 1 shows the study region that includes urban and surrounding non-urban regions of southeastern Virginia. The meteorological stations were selected based on the availability of daily precipitation records and to capture the precipitation patterns in the region. Precipitation occurs both as rainfall and snow; however, the study area received more rainfall and less snow in comparison to other parts of the state. Additionally, tropical storms and hurricanes bring a substantial amount of rainfall to this area. The urban areas in southeastern Virginia experience an average of 1200 mm precipitation each year. The record shows below average precipitation (< 1200 mm) at Norfolk and Hampton, whereas there is above average precipitation (> 1200 mm) at Suffolk and Williamsburg. The Norfolk and Hampton regions are low-lying coastal lands and are vulnerable to floods and sea level rise. The increased frequency of extreme precipitation events and enhanced floods can be exacerbated due to the cascading effects of climate change.

Observed Precipitation of the National Center for Environmental Information

Precipitation records for this study were obtained from the GHCN-D-based stations of the National Center for Environmental Information (NCEI). The stations were selected based on the period of record and these stations had an approximate long-term daily historical time series for

1950-2010 (Table 1). The quality of the data was evaluated using quality assurance reviews and checks for spurious changes in the mean, variance, and outliers from both serial and spatial perspectives (Menne at. al., 2012). These datasets were found to be suitable for both fundamental and applied hydrological analysis at various spatial scales and were previously employed in a variety of assessment activities including the analysis of climate extremes in North America. The analyses illustrated a variety of climate change indices and tracked large-scale changes in observed daily maximum and minimum temperature across the globe.

Simulated Precipitation of the GCMs

The GCMs were selected based on the availability of CMIP5 MACA output (Abatzoglou, 2013) at a daily time step to evaluate how daily extreme rainfall was captured during the historical period (1950-2005). This dataset was subsequently used to predict the changes in the future precipitation regimes (2016-2099) in several studies (Sridhar et al., 2018; Sridhar and Anderson, 2017). We selected 15 GCMs to address and to get the overall understanding of the extremes while considering the inter-model uncertainties resulting from a range of parameters in simulating precipitation at $1/16^{th}$ degree of spatial resolution. The details of these GCMs are included in Table 2.

Weather Research and Forecasting (WRF) Model

The North American Regional Reanalysis (NARR)-derived course gridded precipitation (resolution of 32.6 km) data was used for dynamic downscaling at a 4-km spatial scale. This downscaling was performed using the WRF model from 1982-2010 over southeastern Virginia at the hourly time scale. The first 3 years were considered a spin-up period to stabilize the model and therefore are not included in the analysis. For the simulation with the WRF model, several

inputs were used including the soil parameters, land cover, and sea surface temperature from the

National Centers for Environmental Prediction (NCEP), the Moderate-Resolution Imaging

Spectroradiometer (MODIS), and the National Oceanic and Atmospheric Administration

(NOAA). The hourly precipitation for every 4 km of resolution from 1985-2010 were analyzed

to capture the extreme precipitation events and determine if there were missing input data for

some years (if data were missing, they were excluded from the analysis).

Variable Infiltration Capacity (VIC) Model

For streamflow simulation, we used the VIC 4.2.a (Liang at al., 1994) version where sub-

grid variability is explicitly defined. This model has been extensively used in our climate change

impact assessment studies in many river basins (Hoekema and Sridhar, 2013; Sridhar et al.,

2013; Kang and Sridhar, 2017). The VIC model simulates the water and energy fluxes by

considering the soil and vegetation parameters, meteorological inputs and vegetation library.

Each vegetation class has different parameterizations, including vegetation type, leaf area index

and other physiological characteristics. The model works on the concept of the average weighted

area by considering the elevation and snow bands and it has three soil layers for water and

energy balance calculations. Surface runoff and infiltration is defined by the variable infiltration

curve (Wood et al., 1992) and thus enables runoff calculations for sub-grid-scale areas. We used

the vegetation and soil parameters developed at 1/16thdegree spatial resolution extracted by

Livneh et al. (2013), Maurer et al. (2002) and Tang et al. (2012). The fraction of the vegetation

type for each grid cell was derived from the University of Maryland's 1-km vegetation

classification (Hansen et al., 2000). We applied the VIC model at 1/16th degree resolution with

the meteorological forcing regridded from daily temperature and precipitation observations for

1915-2011 (Livneh et. al., 2013). The meteorological dataset included the precipitation,

minimum temperature, maximum temperature and wind speed derived from approximately

20,000 NOAA stations. We calibrated the VIC model parameters that included the depth of the

soil layers, maximum base flow, maximum soil moisture and variable infiltration parameter

using Shuffled Complex Evolution (SCE) algorithm. The output from VIC model was used to

setup the Noah-MP model including the estimation of input static and dynamic parameters.

Noah MP Land Surface Model

The Noah land surface model with the multi-parameterization scheme is an improved

version of the baseline Noah LSM (Ek et al., 2003; Niu et al., 2011). Our earlier studies using

the Noah model have proven to perform well for water and energy flux simulations from field

scale (Sridhar and Wedin, 2009; Valayamkunnath et al., 2018) to large scales (Sridhar, 2013;

Jaksa and Sridhar, 2015). The interactive vegetation canopy layer was introduced to compute the

canopy and ground surface temperatures. The choice of multi-parameterization was provided for

the vegetation model (leaf dynamics), stomatal resistance, radiation transfer scheme and scheme

for runoff and groundwater. The schemes mainly include the TOPMODEL (Niu et. al., 2007)

and free drainage scheme (Schaake et al., 1996 for the Noah baseline model) and for this study,

free drainage scheme is used. The semi-tile subgrid scheme plays an important role in calculating

the surface energy balance for vegetation and bare ground separately and improves the radiation

balance. The meteorological forcings include the precipitation and wind speed, which were

similar to those used for VIC LSM. The meteorological forcings at the 1/16th-degree spatial

resolution with daily temporal resolution were used to simulate the Noah MP land surface model.

The other meteorological forcings that included air temperature, shortwave and longwave

radiation, relative humidity and pressure were simulated from VIC's output. Wind direction was

derived from CCMP V2.0 U and V component wind data, which is a combination of cross-

calibrated satellite microwave winds and instrument observations (Wentz et al., 2015). The

model output was available at a 0.25-degree spatial resolution at 10 m height and was regridded

to 1/16th degree spatial resolution. The static input parameters, including the initial soil moisture

content, skin temperature, and snow water equivalent, were derived from the VIC's output. The

vegetation type was extracted from the IGBP MODIS classification (University of Maryland),

whereas the soil type index was derived from the hybrid State Soil Geographic Database

(STATSGO) Food and Agricultural Organization soil texture datasets.

Streamflow routing

Finally, streamflow routing was performed using the stand-alone routing model

(Lohmann et al. 1996), which is based on a unit-hydrograph method that uses daily surface

runoff, baseflow and precipitation to estimate the streamflow at the desired location. The flow

direction and flow accumulation files required for the routing network were developed using a

30-m Digital Elevation Model from SRTM (Shuttle Radar Topography mission). The runoff

generated by the model can be used to assess its correlation with the precipitation data and to

observe the shift in future simulations based on the historical observations.

Statistical Methods

While detecting an association or correlation between any variables refers to trend, the

tests are performed generally to assess whether the trend is increasing, decreasing or periodic in

nature. Ordinary least squares (OLS) is one of the most popular linear regression-based trend

detection technique that has been frequently used for evaluating temporal trends in streamflow

and precipitation (Kroll and Stedinger, 1998). It should be noted that OLS is particularly

sensitive to non-normality and outliers. This was because OLS regression minimizes the

differences between observations and the best-fit straight line (Wilks, 2006). The Theil-Sen slope

estimator is the most popular non-parametric technique, which is an alternative to the parametric

ordinary least square regression. This method efficiently computes trends that are insensitive

to outliers and considered to be more accurate than simple linear regression for skewed and

heteroskedastic data and competes well against least squares even for normally distributed data

in terms of statistical power. When the data meets all of the parametric assumptions, the Theil-

Sen has approximately 91% Pitman efficiency for linear regression, and when the data is very

non-normal and skewed, the Theil-Sen efficiency can exceed 1.27 times that of the linear

regression (Armitage et al., 2002; Helsel and Hirsch, 2002; Sheskin, 2007; Sprent and Smeeton,

2007).

Mann-Kendall (MK) trend analysis is a nonparametric rank-based trend test (Gilbert,

1987) that is robust to non-normality and is less influenced by outliers than the ordinary least

squares regression approach (Helsel and Hirsch, 2002). The test identifies systematic increases or

decreases in the rank of the data points with time. The Mann-Kendall Z statistic provides an

indication of whether an existing trend is increasing or decreasing based on decided probability

of significance. We applied a two sample Kolmogorov–Smirnov (KS) test to quantify distance

between the empirical distribution functions of the two datasets. The null distribution of this

statistic was calculated under the null hypothesis so that the samples are drawn from the same

distribution. In each case, the distributions considered under the null hypothesis were continuous

distributions but were otherwise unrestricted. The correlation between the observational dataset

and the simulated dataset was quantitatively assessed through the Nash-Sutcliffe model

efficiency coefficient.

$$E = 1 - \frac{\Sigma_{t=1}^{T}(Q_m^t - Q_o^t)}{\Sigma_{t=1}^{T}(Q_0^t - \overline{Q_o})} \qquad (1)$$

Where Q_0^t is the mean of the observed discharges, Q_m^t is the modeled discharge and Q_0^t is

observed discharge at time t.

RESULTS AND DISCUSSION

Daily Precipitation

The precipitation characteristics were analyzed for 1950-2010 at nine locations in

southeastern Virginia (Figure 2). These stations showed positive skewness with approximately

60% of the precipitation events at or below the mean daily precipitation. Even though the

magnitudes of mean precipitation were below 50 mm, large precipitation events were as high as

300 mm or more in most locations. While the Hampton Roads region experienced less intense

rainfall (< 200 mm per day), Norfolk experienced as much as 300 mm of daily precipitation

during the period of analysis. The largest precipitation event was recorded at Williamsburg (>

350 mm per day), which is located slightly interior from the coastline and northwest of Hampton

Roads and Norfolk.

Extreme Precipitation Trends

Figure 3 illustrates the annual extreme precipitation trends using daily observation data

for 1950-2010. Increasing trends were persistent across southeastern Virginia although few

locations showed opposite (decreasing) trends. These decreasing trends appeared mostly along

the coastline. Around urban locations, extreme precipitation trend estimates in terms of the TS

slope demonstrated changes in the positive direction that ranged between +0.1 to +0.5 per year,

where OLS overestimated the trends between +0.2 and +0.8 (Table 3). The differences were due to the variation in the methods adopted to derive the precipitation distribution. There were disagreements in the trends and directions between these two methods in which the OLS estimates showed an increase in extreme precipitation at a rate of +0.196, whereas the TS estimator slope estimated little or no decrease (-0.023) in Suffolk. This might be due to the presence of outliers and the unequal variation of precipitation events that influenced the OLS-based estimate to be positive. The same factor might influence the quantification trend of extreme precipitation at Williamsburg, where OLS showed the highest increase and an annual rate of +0.8, whereas the Theil-Sen slope increased by +0.28 annually from 1950 to 2010. The TS estimated the precipitation trend with the highest increase (+0.5) and was located at Suffolk, which was in line with the MK analysis due to a significant increase in the extreme precipitation (Z=1.79). The positive or negative MK trend analysis of the annual extreme daily precipitation agreed with the increase or decrease in the TS trends, respectively. At α=0.05 (95 % confidence level), the computed probability was greater than 0.95 at Suffolk, Wallaceton, Williamsburg and Norfolk (Table 3) which indicates that the trend is said to be decreasing if Z (Mann-Kendall test statistic) is negative and the computed probability is greater than the level of significance (α=0.05) whereas the trend is said to be increasing if Z is positive and the computed probability is greater than the level of significance. In addition to the trends, it was evident that the tails of the distribution of the above-median precipitation showed a wide range. Even though the average of the highest five precipitation events in each location was below 100 mm, the daily precipitation was recorded at greater than 200 mm at Norfolk, Williamsburg, Suffolk, and Hampton. Some of these locations measured as high as 350 mm daily precipitation in several occasions during the period of analysis.

Extreme Precipitation Intensity and Frequency

When the annual high precipitation events, based on higher than the 90th percentile distribution, were compared with low precipitation events of less or equal to 90th percentile distribution, all of the locations showed a precipitation ratio range between 5-10 times (Figure 4). However, these ratios showed a distinct increase during the last 10 to 15 years around the urban areas of Hampton, Norfolk, and Williamsburg. Regardless of the high ratio in recent years, these high precipitation events were consistently more than 10 times every year from 1950-2010 (indicated by blue line in Figure 4). Although few locations along the coastline showed a decreasing amount of high precipitation events, the majority of the locations agreed with the increased precipitation ratio during the period of analysis. In the last few years after 2001, where most of the locations showed a high frequency of extreme precipitation, the Hampton region experienced less intense rainfall (ratio < 10). The regions, including Suffolk and Williamsburg, were susceptible to the most frequent extreme precipitation, which was over 300 mm (at its highest) compared to the other regions in southeastern Virginia.

Comparison of Annual and Seasonal Extreme Precipitation

The *in situ* daily observation of the annual extreme precipitation for nine locations was compared with downscaled precipitation for 1950-2005 to illustrate the ability of the downscaled GCMs in capturing the extreme precipitation events (Figure 5). The hourly precipitation extremes from WRF simulations were also compared to evaluate the ability of the WRF model in simulating high-resolution precipitation for the same locations. The comparisons showed that the ensemble of extreme precipitation events of the GCMs captured almost all of the events with a wide range of uncertainty. At most locations, GCMs were overpredicting annual precipitation

extremes, and a very few events remained uncaptured. The seasonality in the extreme

precipitation was well-captured by the ensemble of the downscaled GCMs; however, the WRF-

NARR-based seasonal distribution of extreme precipitation events were not able to statistically

correlate (Table 4). The distribution statistics of the simulated mean extreme precipitation of 15

GCMs were within the critical distribution estimates (based on KS lookup table) in most

locations. Simulated extreme precipitation was able to generate a similar seasonal extreme

precipitation distribution compared to that of the observations for all of the locations except

Holland, West Point, and Williamsburg. At these locations, the underprediction of seasonal

extreme precipitation by the GCMs caused a difference in precipitation distribution when

compared with seasonal observations. Assuming a 5% significance level, the distribution of the

mean extreme daily precipitation of 15 GCMs relative to extreme annual observations, the

distribution estimated significant difference in most locations showing higher KS distribution

statistics than the critical distribution (Table 4a). This was due to the presence of several annual

extreme events that were not captured by the mean of the simulated annual extreme precipitation.

The mean of the simulated annual extreme daily precipitation distribution statistically matched

with the extreme of the observed data at Hampton and Suffolk.

The overprediction by the GCMs caused minimal deviations from the annual extreme

daily observation. The KS distribution statistics also revealed that incorporated hourly simulated

precipitation from WRF-NARR extreme daily precipitation were also unable to match observed

the daily extreme precipitation distribution as several extreme observations were underpredicted

between 1985-2010 (Table 4b). The mean of the downscaled annual extreme daily precipitation

showed an average deviation of 15% with the observed extremes, which resulted from the

underprediction of the extreme precipitation at all of the locations. The deviations were larger

(>20%) for Holland, Wallaceton, and West point. The mean deviation at the Hampton region

was only 1%, whereas it was approximately 3% at Suffolk. When the deviations of the annual

extreme daily precipitation by GCMs were computed at nine locations, the least bias was evident

from two models, GFDL-ESM2M (10.61%) and BCC-CSM1-1-m (11.56%) (Table 5).

Trends and Distribution of Future Daily Maximum Precipitation

From the analysis of two downscaled GCMs (BCC-CSM1-1-m and GFDL-ESM2M),

both the frequency and magnitude of the extreme precipitation in the RCP 4.5 and RCP 8.5

scenarios were found to increase in comparison with historical observations (Figure 6). In both

RCP scenarios, annual extreme daily precipitation was much higher in comparison to the

corresponding mean and median. RCP 8.5 scenario showed high frequency and magnitude at all

nine locations, however, there were several extreme precipitation events that were predicted

higher in RCP 4.5 scenario. At Suffolk, West Point, and Williamsburg, where high daily

precipitation (~300 mm) were recorded for the historical period, the extreme precipitation was

predicted over 400 mm in several occasions during the period of 2016-2099. These estimates of

magnitude were almost twice the historical records with regard to the annual extreme daily

precipitation events.

The frequency of these precipitation events showed increases in the future. In both RCP

scenarios, these three locations (Suffolk, West Point and Williamsburg) predicted nearly 100

events where the precipitation was expected to be higher than 400 mm. Even with a decreased

precipitation trend in the RCP 4.5 scenario in these three locations, precipitation magnitudes

higher than 400 mm were estimated to occur more than 32 times in the future.

These increases in frequency and magnitude were also expected to change the

precipitation distribution in the future where statistically significant differences were noted with

the historical observations (Table 6). The KS test analysis estimated a different distribution (*D-statistical > D-critical*) in the annual extreme precipitation at all locations in comparison to the historical period, although the seasonal extreme distribution might be similar at very few locations (*D-statistical < D-critical*). The KS analysis for extreme precipitation predicted a similar statistical distribution at Norfolk; however, statistical differences were expected at Hampton. The frequency and magnitude of the future extreme precipitation events at Hampton and Norfolk were also expected to increase despite decreasing (RCP 4.5) or increasing (RCP 8.5) prediction trends by the scenarios. When both RCP scenarios were considered, it was predicted that the Hampton region was expected to experience 6 to 19 precipitation events that would be higher than 400 mm, whereas the Norfolk region was predicted to have 3 to 10 similar precipitation events from 2016-2099.

Spatial Analysis of Precipitation

Figure 7 shows the extreme precipitation distribution extracted from the downscaled GCMs for 1950-2099 over southeastern Virginia at nine locations. Both the spatial and temporal distribution (Figure 10) of precipitation for the historical period agreed well over most locations. Despite the underestimation (Williamsburg, Suffolk) or overestimation (Hampton), the zones for annual extreme daily precipitation events across the study region were well identified. Future extreme precipitation events over these areas also showed similar patterns. Simulated precipitation from two GCMs (BCC-CSM1-1-m and GFDL-ESM2M) predicted increased frequency and magnitude from 2016-2099. As expected, the RCP 8.5 scenario projected high precipitation extremes compared to that of the RCP 4.5 scenario. The BCC-CSM1-1-m model predicted annual extreme daily precipitation in the southern region, which ranged between 450-

700 mm. The Williamsburg region even predicted 2-3 times higher magnitudes (> 700 mm) than

the historical period. However, the GFDL-ESM2M model predicted less intense precipitation at

the RCP 4.5 scenario ranging between 300 and 450 mm (1~2 times of the historical precipitation

events) in most locations. However, the GFDL-ESM2M model in the RCP 8.5 scenario predicted

450 to 700 mm of precipitation across the study region. At the Hamptons and depending on the

location, the RCP 4.5 scenario projected an increase of 1.5 to 2 times, whereas the RCP 8.5

scenario expected an increase of 2.0 to 3.0 times of the annual extreme daily precipitation.

Depth-Duration-Return Period Assessment

The annual extreme daily precipitation observations and estimates were used to highlight

flood frequencies for 24- and 48-hour durations at nine locations (Figure 8). The comparison for

1950-2005 showed that longer duration generally predicted a high precipitation and return period

except at two locations along the coastline. Both the Norfolk and Virginia Beach region

illustrated high precipitation intensity for high return periods over a duration of 24 hours of

rainfall. When the GCMs were used to reproduce flood frequencies for the historical period

(1950-2005), both 24- and 48-hour extreme rainfall deviated in most locations. However, these

deviations were higher for 24 hours than that of the 48-hour durations. Despite these deviations,

the extreme precipitation at the Hampton, Norfolk, Virginia Beach and West point regions were

well captured.

When the same GCMs were used to predict climate change impacts on precipitation

extremes for 2016-2099, the RCP 8.5 scenario projected higher precipitation relative to the RCP

4.5 scenario in most locations. The distinct differences in the prediction were observed at West

point and Williamsburg, which are the regions with high precipitation. These regions were also

found to be vulnerable to frequent floods in the future. The increased intensity and frequency in

precipitation at Hampton and Norfolk were expected to cause moderate flooding in the future.

For most regions, the increase in the precipitation intensity for RCP 4.5 was estimated to be two

times whereas for RCP 8.5 it was estimated to increase by three times compared to historical

period. Exceptionally, Norfolk shows relatively less increase in precipitation intensity, which

was estimated to be 1.5 times for RCP 4.5 and 2 times for RCP 8.5. In case of Hampton, the

increase in duration of intense precipitation events (48 hr) was indicative whereas the predicted

precipitation intensity was only 1.06 and 1.08 times for the RCP 4.5 and RCP 8.5 scenarios

relative to the historical period. An intercomparison between Norfolk and Hampton reveals that

precipitation intensity for the Norfolk regions is expected to increase around 1.1 times and 1.6

times in the RCP 4.5 and RCP 8.5 scenarios when compared to the Hampton region for the

historical period of analysis.

Streamflow Calibration and Validation

To assess how extreme precipitation might impact streamflow, we simulated flows in a

hydrological modeling framework with VIC and Noah MP models. We used the United States

Geological Survey (USGS) streamflow data to calibrate and validate the VIC and Noah MP land

surface model. Figure 9 (a) shows the gauging stations in the James River Basin in the

downstream section of the James River. There were no stations near the coastal region, and

hence this area was chosen to obtain a better idea about the watershed response to varying

precipitation regimes. We calibrated and validated the streamflow data obtained from the

combination of VIC and Noah MP results with the USGS monthly statistics and extended this

information to simulate flows from Hampton, Suffolk, Williamsburg and Virginia Beach where

there were no observed flow data. Three parameters were calibrated to improve the performance

of the model based on Cai et al. (2014) that included saturated soil conductivity (SATDK),

maximum soil moisture content (MAXSMC) and function of soil type (BB). During the

calibration period (1991-2000), the NSE calculated for monthly streamflow was 0.81 at the

USGS gauge station (Figure 9a). Similar performance can be noted for the validation period with

an NSE of 0.84 (Figure 9b).

Projected streamflow

With the calibration parameters, we simulated future streamflow based on the MACA

datasets for two GCM's (BCC-CSM1.1 and CanESM2) for the historical as well as the future

period with GCMs and at a spatial resolution of 1/16th degree. Figure 10 indicates the annual

streamflow rate (ft^3/s) and total precipitation (cm) for different locations from 2006-2097. There

is not much variation in highflows over time but a shift in peaks were evident for the two RCPs.

In the case of RCP 4.5, increased discharge rates were found between 2028-2040 for the BCC-

CSM1.1 model, whereas in the case of CanESM2, it was found to be increasing between 2016-

2028 at all selected locations including the USGS gauge stations (Figure 3). In the case of RCP

8.5, increased discharge rates were found to occur around the mid-century for CanESM2 and

after mid-century for BCC-CSM1.1.

Flood frequency Assessment

Figure 11 highlights the changes in flood frequency over the future period (2006-2099)

compared to the baseline period (1950-2016). The figure includes the flood frequency curves for

all selected locations, including the USGS gauge station, and the GCMs show an overall increase

in the magnitude of highflows. The RCP 4.5 scenario predicted a decrease in the mean flood

magnitude compared to the baseline period (red points), whereas RCP 8.5 showed a consistent

increase in mean flood magnitude at all of the selected locations. The flood frequency curves at

the USGS gauge station indicate an increase of up to 50% in flood magnitude. Similarly,

Williamsburg and Hampton showed an increase in flood magnitudes. While the uncertainties

between the GCMs resulted in differences in precipitation, and hence in streamflow simulated by

the hydrology models, the calibration exercise accounts for these uncertainties provided there are

opportunities to estimate relative changes between historic and future periods. Figure 11 also

highlights the climate changing effects on flood frequency curve with a specific focus on the

James River basin. However, future research for neighboring catchments is necessary to clearly

understand the impacts of climate change in the Southeastern Virginia.

CONCLUSION

The analysis of the spatiotemporal characteristics of precipitation is important to

understand its influences for the urban environment. It is important to understand the extreme

precipitation characteristics in urban areas for applications such as flood monitoring and

designing of drainage infrastructure. Extreme precipitation can be devastating in the built

environment as the fraction of impervious areas increase and thus aggravate the flooding

potential. The uncertainties are associated with the changing climate and are due to the

limitations of records and climate models to capture extreme precipitation. This study focused on

quantitative analysis to understand the pattern of historical precipitation extremes and to evaluate

projected precipitation in a changing climate in southeastern Virginia, which is the base for

national security establishments. The temporal and spatial characteristics of observed extreme

precipitation and GCM projections were investigated to characterize the changes in precipitation

and the corresponding streamflow magnitudes for 1950-2099. These extreme precipitation

magnitudes were above 300 mm in many events, whereas the mean and median of the

precipitation events was below 50 mm.

The analysis of the daily observation of precipitation using parametric (OLS) and

nonparametric (Theil-Sen slope estimator, Mann-Kendall Test, Kolmogorov-Smirnov test)

statistical techniques at a confidence level of $p \leq 0.05$ identified the overall increases in extreme

precipitation in the study area. The main areas of extreme precipitation were concentrated in a

few urban regions, including Williamsburg, Suffolk, and Norfolk, due to extreme precipitation

projections in the summer months.

Comparisons between MACA-based downscaled daily precipitation from 15 GCMs and

WRF-NARR-based downscaled hourly precipitation simulation were made to understand the

extreme spatial and temporal characteristics. The magnitude and frequency of the annual extreme

precipitation were not consistent across multiple locations. There were a few observation sites

where the annual extreme precipitation was almost twice as much when compared with other

sites. The mean or median of 15 annual extreme precipitation simulations was generally

consistent; however, a few extreme events of major concern were underestimated at each site.

These differences were attenuated when seasonal extreme precipitation was evaluated where the

uncertainty was less. It should be noted that increased temporal resolution in the WRF-based

NARR precipitation extremes were not able to simulate the extreme precipitation events.

However, a number of GCMs, when engaged to capture these extremes, showed that the

estimations were reasonable with some degree of uncertainty.

The frequencies of these extreme precipitation events might also increase in the future (2016-2099). The statistical metrics revealed that future precipitation magnitudes could be 2 to 3 times greater relative to the historical period of analysis. These extreme precipitation events are crucial for the proper design of urban drainage and stormwater infrastructure systems. Simulated streamflow for the lower James River Basin suggested that both RCP scenarios projected higher peaks in the downstream sections. The flood frequency also indicated an increase of up to 50% in flood magnitude over the basin including Williamsburg and Hampton. The extreme precipitation analysis from downscaled GCMs combined with a hydrological modeling assessment can serve as a guiding tool in estimating non-stationary future flood frequencies and this can be useful for designing urban stormwater infrastructure.

Acknowledgments

LITERATURE CITED

Abatzoglou, J.T., 2013. Development of Gridded Surface Meteorological Data for Ecological Applications and Modelling. *International Journal of Climatology* 33(1): 121-131. https://doi.org/10.1002/joc.3413.

Alam, M.S. and A. Elshorbagy, 2015. Quantification of the Climate Change-induced Variations in Intensity–Duration–Frequency Curves in the Canadian Prairies. *Journal of Hydrology* 527: 990-1005. https://doi.org/10.1016/j.jhydrol.2015.05.059.

Ali, H., & V. Mishra, (2018). Increase in Subdaily Precipitation Extremes in India Under 1.5 and 2.0° C Warming Worlds. *Geophysical Research Letters*, *45*(14), 6972-6982. https://doi.org/10.1029/2018GL078689

Arnbjerg-Nielsen, K.,2012. Quantification of climate change effects on extreme precipitation used for high resolution hydrologic design, *Urban Water Journal*, 9(2), 57-65

Armitage, P., G. Berry, and J.N.S. Matthews, 2008. Statistical Methods in Medical Research (4th edition). John Wiley & Sons.

Arriaga-Ramírez, S. and T. Cavazos, 2010. Regional Trends of Daily Precipitation Indices in Northwest Mexico and Southwest United States. *Journal of Geophysical Research: Atmospheres* 115(D14). https://doi.org/10.1029/2009JD013248.

Brown, L. R. (2001). *State of the World, 2001: A Worldwatch Institute Report on Progress Toward a Sustainable Society*. WW Norton & Company.

Cai, X., Z.L. Yang, C.H. David, G.Y. Niu, and M. Rodell, 2014. Hydrological Evaluation of the Noah-MP Land Surface Model for the Mississippi River Basin. *Journal of Geophysical Research: Atmospheres*, *119*(1): 23-38. https://doi.org/10.1002/2013JD020792.

Camici, S., L. Brocca, F. Melone, and T. Moramarco, 2013. Impact of Climate Change on Flood Frequency using Different Climate Models and Downscaling Approaches. *Journal of Hydrologic Engineering* 19(8): p.04014002. https://doi.org/10.1061/(ASCE)HE.1943-5584.0000959.

Chen, L. and O.W. Frauenfeld, 2014. A Comprehensive Evaluation of Precipitation Simulations over China based on CMIP5 Multimodel Ensemble Projections. *Journal of Geophysical Research: Atmospheres* 119(10): 5767-5786. https://doi.org/10.1002/2013JD021190.

Crétat, J., E.K. Vizy, and K.H. Cook, 2014. How Well are Daily Intense Rainfall Events Captured by Current Climate Models over Africa?. *Climate dynamics* 42(9-10): 2691-2711. 10.1007/s00382-013-1796-7.

Denault, C., R.G. Millar, and B.J. Lence, 2002. Climate Change and Drainage Infrastructure Capacity in an Urban catchment. In Proc. Annual Conference of the Canadian Society for Civil Engineering (Vol. 5, No. 6).

Ek, M.B., K.E. Mitchell, Y. Lin, E. Rogers, P. Grunmann, V. Koren, G. Gayno, and J.D. Tarpley, 2003. Implementation of Noah Land Surface Model Advances in the National Centers for Environmental Prediction Operational Mesoscale Eta model. *Journal of Geophysical Research: Atmospheres 108*(D22). https://doi.org/10.1029/2002JD003296.

Gilbert, R.O., 1987. Statistical Methods for Environmental Pollution Monitoring. John Wiley & Sons. pp. 320.

Groisman, P.Y. and D.R. Easterling, 1994. Variability and Trends of Total Precipitation and Snowfall over the United States and Canada. *Journal of Climate* 7(1): 184-205. https://doi.org/10.1175/1520-0442(1994)007<0184:VATOTP>2.0.CO;2

Hansen, M. C., R. S. Defries, J. R. G. Townshend, and R. Sohlberg, 2000. Global land cover classification at 1 km spatial resolution using a classification tree approach, *Remote Sens. Environ.*, 21, 1331–1364.

Helsel, D.R. and R.M. Hirsch, 2002. Statistical Methods in Water Resources (Vol. 323). Reston, VA: US Geological Survey.

Hoekema, D. J., V. Sridhar, 2013. A system dynamics model for conjunctive management of water resources in the Snake River basin, Journal of the American Water Resources Association, Vol 49, No. 6: 1327-1350, DOI: 10.1111/jawr.12092.

Hofstra, N., M. Haylock, M. New, and P.D. Jones, 2009. Testing E-OBS European High-Resolution Gridded Dataset of Daily Precipitation and Surface Temperature. *Journal of Geophysical Research: Atmospheres* 114(D21). https://doi.org/10.1029/2009JD011799.

Jaksa, W.T.A., V. Sridhar, 2015. Effect of irrigation in simulating long-term evapotranspiration climatology in a human-dominated river basin system, Agricultural and Forest Meteorology, 200, 109-118, DOI: 10.1016/j.agrformet.2014.09.008.

Kang, H., V. Sridhar, 2017. Assessment of future drought conditions in the Chesapeake Bay watershed, Journal of the American Water Resources Association, DOI: 10.1111/1752-1688.12600.

Karl, T.R. and R.W. Knight, 1998. Secular Trends of Precipitation Amount, Frequency, and Intensity in the United States. *Bulletin of the American Meteorological society* 79(2): 231-241. https://doi.org/10.1175/1520-0477(1998)079<0231:STOPAF>2.0.CO;2.

Khaliq, M.N., T.B. Ouarda, P. Gachon, L. Sushama, and A. St-Hilaire, 2009. Identification of Hydrological Trends in the Presence of Serial and Cross Correlations: A Review of Selected Methods and their Application to Annual Flow Regimes of Canadian Rivers. *Journal of Hydrology* 368(1-4): 117-130. https://doi.org/10.1016/j.jhydrol.2009.01.035.

Kroll, C.N., J.R. Stedinger, 1998. Regional hydrologic analysis: Ordinary and generalized least squares revisted. *Water Resources Research*, 34 (1), 121-128.

Liang, X., D.P. Lettenmaier, E.F. Wood, and S.J. Burges, 1994. A Simple Hydrologically Based Model of Land Surface Water and Energy Fluxes for General Circulation Models. *Journal of Geophysical Research: Atmospheres* 99(D7):14415-14428.

Liew, S.C., S.V. Raghavan, and S.Y. Liong, 2014. How to Construct Future IDF Curves, under Changing Climate, for Sites with Scarce Rainfall Records?. *Hydrological processes* 28(8): 3276-3287. https://doi.org/10.1002/hyp.9839

Livneh B., E.A. Rosenberg, C. Lin, B. Nijssen, V. Mishra, K.M. Andreadis, E.P. Maurer, and D.P. Lettenmaier, 2013. A Long-Term Hydrologically Based Dataset of Land Surface Fluxes and

States for the Conterminous United States: Update and Extensions, *Journal of Climate* 26: 9384–9392. https://doi.org/10.1175/JCLI-D-12-00508.1.

Lohmann, D., Nolte-Holube, R., and E. Raschke, 1996. A Large-scale Horizontal Routing Model to be Coupled to Land Surface Parametrization Schemes. *Tellus A* 48(5): 708-721.

Maurer, E.P., A.W. Wood, J.C. Adam, D.P. Lettenmaier, and B. Nijssen, 2002. A Long-term Hydrologically Based Dataset of Land Surface Fluxes and States for the Conterminous United States. Journal of climate, 15(22): 3237-3251. https://doi.org/10.1175/1520-0442(2002)015<3237:ALTHBD>2.0.CO;2.

Maurer, E.P., G. Kayser, L. Doyle, A.W. Wood, 2018. Adjusting Flood Peak Frequency Changes to Account for Climate Change Impacts in the Western United States, *Journal of Water Resources Planning and Management* 144(3): 05017025. https://doi.org/10.1061/(ASCE)WR.1943-5452.0000903.

McAfee, S.A., G. Guentchev, and J.K. Eischeid, 2013. Reconciling Precipitation Trends in Alaska: 1. Station-based Analyses. *Journal of Geophysical Research: Atmospheres* 118(14): 7523-7541. https://doi.org/10.1002/jgrd.50572

McAfee, S.A., G. Guentchev, and J.K. Eischeid, 2014. Reconciling Precipitation Trends in Alaska: 2. Gridded Data Analyses. *Journal of Geophysical Research: Atmospheres* 119(24): 13-820. https://doi.org/10.1002/2014JD022461.

Menne, M. J., I. Durre, R. S. Vose, B. E. Gleason, & T. G. Houston, 2012. An overview of the global historical climatology network-daily database. *Journal of Atmospheric and Oceanic Technology*, *29*(7), 897-910. https://doi.org/10.1175/JTECH-D-11-00103.1

Min, S.K., X. Zhang, F.W. Zwiers, and G.C. Hegerl, 2011. Human Contribution to More-intense Precipitation Extremes. *Nature* 470(7334): 378. 10.1038/nature09763.

Mishra, V. and D.P. Lettenmaier, 2011. Climatic Trends in Major US Urban Areas, 1950–2009. *Geophysical Research Letters* 38(16): L16401. https://doi.org/10.1029/2011GL048255.

Mishra, V., A.R. Ganguly, B. Nijssen, and D.P. Lettenmaier, 2015. Changes in Observed Climate Extremes in Global Urban Areas. *Environmental Research Letters* 10(2): 024005. doi:10.1088/1748-9326/10/2/024005.

Mukherjee, S., S. Aadhar, D. Stone, & V. Mishra, 2018. Increase in extreme precipitation events under anthropogenic warming in India. *Weather and Climate Extremes*. https://doi.org/10.1016/j.wace.2018.03.005

Niu, G.Y., Z.L. Yang, R.E. Dickinson, L.E. Gulden, and H. Su, 2007. Development of a Simple Groundwater Model for Use in Climate Models and Evaluation with Gravity Recovery and Climate Experiment Data. *Journal of Geophysical Research: Atmospheres 112*(D7). https://doi.org/10.1029/2006JD007522

Niu, G.Y., Z.L. Yang, K.E. Mitchell, F. Chen, M.B. Ek, M. Barlage, A. Kumar, K. Manning, D. Niyogi, E. Rosero, and M. Tewari, 2011. The Community Noah Land Surface Model with Multiparameterization Options (Noah-MP): 1. Model description and evaluation with local-scale measurements. *Journal of Geophysical Research: Atmospheres* 116(D12). https://doi.org/10.1029/2010JD015139.

Osborn, T.J., M. Hulme, P.D. Jones, and T.A. Basnett, 2000. Observed Trends in the Daily Intensity of United Kingdom Precipitation. *International Journal of Climatology* 20(4): 347-364.

Rosenzweig, C., W. Solecki, S.A. Hammer, and S. Mehrotra, 2010. Cities lead the way in climate–change action. *Nature* 467(7318): 909. doi: 10.1038/467909a.

Schaake, J.C., V.I. Koren, Q.Y. Duan, K. Mitchell, and F. Chen, 1996. Simple Water Balance Model for Estimating Runoff at Different Spatial and Temporal Scales. *Journal of Geophysical Research: Atmospheres*, *101*(D3), 7461-7475. https://doi.org/10.1029/95JD02892.

Sen Roy, S. and R.C. Balling, 2004. Trends in Extreme Daily Precipitation Indices in India. *International Journal of climatology* 24(4): 457-466. doi:10.1002/joc.995.

Sheskin, D., 2007. Handbook of Parametric and Nonparametric Statistical Procedures (4th Ed.). Boca Raton, FL, USA: Chapman & Hall/CRC.

Solomon, S., D. Qin, M. Manning, Z. Chen, M. Marquis, K.B. Averyt, M. Tignor, and H.L. Miller, 2007. IPCC, Climate Change 2007: the Physical Science Basis. Contribution of Working Group I to the Fourth Assessment Report of the Intergovernmental Panel on Climate Change. 98-101.

Sprent, P. and N.C. Smeeton, 2007. Applied Nonparametric Statistical Methods. CRC Press.

Sridhar, V., D. A. Wedin, 2009. Hydrological behavior of Grasslands of the Sandhills: Water and Energy Balance Assessment from Measurements, Treatments and Modeling, Ecohydrology, 2, 195-212, DOI:10.1002/eco.61.

Sridhar, V., 2013. Tracking the influence of irrigation on land surface fluxes and boundary layer climatology, Journal of Contemporary Water Research & Education, 152, 79-93.

Sridhar, V., X. Jin, W.T. Jaksa, 2013. Explaining the hydroclimatic variability and change in the Salmon River basin, Climate Dynamics, 40, 1921–1937, DOI 10.1007/s00382-012-1467-0.

Sridhar, V., K.A. Anderson, 2017. Human-induced modifications to boundary layer fluxes and their water management implications in a changing climate, Agricultural and Forest Meteorology, 234, 66-79, DOI:10.1016/j.agrformet.2016.12.009.

Sridhar, V., M. M. Billah, J. Hildreth, 2018. Development of a coupled surface and groundwater hydrological model (VIC-MODFLOW) and evaluation in the Snake River Basin, Groundwater, DOI:10.1111/gwat.12610.

Tang, Q., E.R. Vivoni, F. Muñoz-Arriola, and D.P. Lettenmaier, 2012. Predictability of Evapotranspiration Patterns using Remotely Sensed Vegetation Dynamics during the North American Monsoon. *Journal of Hydrometeorology* 13(1): 103-121. https://doi.org/10.1175/JHM-D-11-032.1.

Valayamkunnath, P., V. Sridhar, W. Zhao, R. G. Allen, 2018. Intercomparison of surface energy fluxes, soil moisture, and evapotranspiration from eddy covariance, large aperture scintillometer, and modeling across three ecosystems in a semiarid climate, Agricultural and Forest Meteorology, 248, 22-47, DOI: 10.1016/j.agrformet.2017.08.025.

Wentz, F.J., J. Scott, R. Hoffman, M. Leidner, R. Atlas, and J. Ardizzone, 2015. Remote Sensing Systems Cross-Calibrated Multi-Platform (CCMP) 6-hourly ocean vector wind analysis product on 0.25 deg grid, Version 2.0. Remote Sensing Systems, Santa Rosa, CA.

Wilks, D.S., 2006. Statistical Methods in the Atmospheric Sciences, Int. Geophys. Ser., 2nd ed., vol. 91, edited by R. Dmowska, D. Hartmann and H. T. Rossby, Academic Press, Burlington, MA.

Wood, E.F., D.P. Lettenmaier, and V.G. Zartarian, 1992. A Land-surface Hydrology Parameterization with Subgrid Variability for General Circulation Models. *Journal of Geophysical Research: Atmospheres 97*(D3), 2717-2728. https://doi.org/10.1029/91JD01786.

World Health Organization, 2014. Global status Report on Alcohol and Health-2014. World Health Organization. (www.who.int/substance_abuse/publications/global_alcohol_report/en/)

Wuebbles, D.J., K. Kunkel, M. Wehner, and Z. Zobel, 2014. Severe Weather in United States Under a Changing Climate, *EOS, Transactions* 95, 18: 149-150. https://doi.org/10.1002/2014EO180001.

TABLE 1. A list of the *in situ* observation station of the Global Historical Climatology Network (GHCND) for precipitation trend analysis for 1950-2010.

Station	Name of the stations	Elevation (m)	Latitude	Longitude
Holland	Holland 1 E VA US	24.1	36.6833	-76.7833
Suffolk	Suffolk Lake Kilby VA US	6.1	36.7333	-76.6000
Wallaceton	Wallaceton Lake Drummond VA US	9.1	36.6000	-76.4333
West Point	West point 2 NW VA US	6.1	37.5167	-76.8167
Williamsburg	Williamsburg 2 N VA US	21.0	37.2667	-76.7000
Hampton	Langley Air Force base VA US	3.0	37.0833	-76.3500
Norfolk Airport	Norfolk International Airport VA US	11.9	36.8833	-76.2000
Norfolk	Norfolk NAS VA US	6.1	36.9375	-76.2893
Oceana	Oceana NAS VA US	7.0	36.8333	-76.0333

TABLE 2. A list of the Global Climate Models (GCMs) of the Coupled Model Intercomparison Project 5 (CMIP5) that are downscaled using Multivariate Adaptive Constructed Analogs (MACA) techniques for precipitation trend analysis for 1950-2099.

Model	Model Country	Model Agency	Spatial Resolution
BCC-CSM1-1	China	Beijing Climate Center, China Meteorological Administration	$1/16^{th}$ of a degree
BCC_CSM1-1-m	China	Beijing Climate Center, China Meteorological Administration	$1/16^{th}$ of a degree
BNU-ESM	China	College of Global Change and Earth System Science, Beijing Normal University, China	$1/16^{th}$ of a degree
CanESM2	Canada	Canadian Centre for Climate Modeling and Analysis	$1/16^{th}$ of a degree
CCSM4	USA	National Center of Atmospheric Research, USA	$1/16^{th}$ of a degree
CNRM-CM5	France	National Centre of Meteorological Research, France	$1/16^{th}$ of a degree
CSIRO-Mk3-6-0	Australia	Commonwealth Scientific and Industrial Research Organization/Queensland Climate Change Centre of Excellence, Australia	$1/16^{th}$ of a degree
GFDL-ESM2M	USA	NOAA Geophysical Fluid Dynamics Laboratory, USA	$1/16^{th}$ of a degree
GFDL-ESM2G	USA	NOAA Geophysical Fluid Dynamics Laboratory, USA	$1/16^{th}$ of a degree
INM-CM4	Russia	Institute for Numerical Mathematics, Russia	$1/16^{th}$ of a degree
IPSL-CM5A-LR	France	Institut Pierre Simon Laplace, France	$1/16^{th}$ of a degree
IPSL-CM5A-MR	France	Institut Pierre Simon Laplace, France	$1/16^{th}$ of a degree
IPSL-CM5B-LR	France	Institut Pierre Simon Laplace, France	$1/16^{th}$ of a degree
MIROC5	Japan	Atmosphere and Ocean Research Institute (The University of Tokyo), National Institute for Environmental Studies, and Japan Agency for Marine-Earth Science and Technology	$1/16^{th}$ of a degree
MIROC-ESM	Japan	Japan Agency for Marine-Earth Science and Technology, Atmosphere and Ocean Research Institute (The University of Tokyo), and National Institute for Environmental Studies	$1/16^{th}$ of a degree

TABLE 3. An estimation of the slope of the precipitation trends using linear regression, the Theil-Sen estimator, and Mann-Kendall analysis for 1950-2010. The significant trends at few locations are indicated in italics.

Station	Linear Regression	Theil-Sen Estimator	Mann-Kendell Analysis		
	Slope	Slope	Test Z	p-value	Trend (α=0.05)
Holland	0.196	-0.023	-0.06	0.476078	-
Suffolk	0.799	0.491	1.79	0.963273	+
Wallaceton	0.448	0.252	1.31	0.904902	-
West Point	0.198	0.100	0.79	0.785236	-
Williamsburg	0.821	0.279	1.44	0.925066	-
Hampton	-0.021	-0.125	-0.46	0.322758	-
Norfolk Airport	0.340	0.152	0.46	0.677242	-
Norfolk	0.509	0.239	1.31	0.904902	-
Oceana	-0.203	-0.175	-1.23	0.109349	-

TABLE 4a. An estimation of the precipitation distribution between GCMs and GHCND *in situ* observation using Kolmogorov-Smirnov test analysis for 1950-2005.

	Seasonal Extreme Daily Precipitation		Annual Extreme Daily Precipitation	
	D-statistics	*D-critical*	*D-statistics*	*D-critical*
Holland	0.049	0.029	0.049	0.029
Suffolk	0.070	0.028	0.070	0.028
Wallaceton	0.057	0.030	0.057	0.030
West Point	0.044	0.031	0.044	0.031
Williamsburg	0.065	0.028	0.065	0.028
Hampton	*0.024*	*0.029*	*0.024*	*0.029*
Norfolk Airport	0.030	0.028	0.030	0.028
Norfolk	0.072	0.024	0.072	0.024
Oceana	0.049	0.029	0.049	0.029

TABLE 4b. An estimation of the precipitation distribution between NARR-WRF and GHCND *in situ* observation using Kolmogorov-Smirnov test analysis for 1985-2010.

	Seasonal Extreme Daily Precipitation		Annual Extreme Daily Precipitation	
	D-statistics	*D-critical*	*D-statistics*	*D-critical*
Holland	0.113	0.044	0.082	0.034
Suffolk	0.102	0.043	0.068	0.034
Wallaceton	0.195	0.043	0.069	0.033
West Point	0.068	0.045	0.073	0.035
Williamsburg	0.105	0.043	0.050	0.033
Hampton	0.121	0.047	0.110	0.041
Norfolk Airport	0.081	0.043	0.085	0.034
Norfolk	0.065	0.015	0.120	0.033
Oceana	0.061	0.043	0.090	0.034

TABLE 5. An estimation of the daily precipitation statistics indicating -percent bias between downscaled precipitation of CMIP5 models and GHCND *in situ* observation for 1950-2005.

Model	Mean % Bias
BCC-CSM1-1	16.23
BCC-CSM1-1-m	**11.56**
BNU-ESM	13.80
CanESM2	15.54
CCSM4	23.32
CNRM-CM5	16.84
CSIRO-Mk3-6-0	19.12
GFDL-ESM2M	**10.61**
GFDL-ESM2G	18.41
INM-CM4	21.29
IPSL-CM5A-LR	15.99
IPSL-CM5A-MR	14.26
IPSL-CM5B-LR	15.37
MIROC5	20.63
MIROC-ESM	14.97
WRF-NARR	19.73

TABLE 6. Comparison of extreme precipitation distribution using CMIP5 MACA RCP 4.5 and 8.5 scenarios with GHCND observation using Kolmogorov-Smirnov test analysis for 2016-2099.

	Annual Extreme Daily Precipitation				Seasonal Extreme Daily Precipitation			
Station ID	D_{45}-*statistics*	D_{45}-*critical*	D_{85}-*statistics*	D_{85}-*critical*	D_{45}-*statistics*	D_{45}-*critical*	D_{85}-*statistics*	D_{85}-*critical*
Holland	0.226	0.021	0.231	0.020	0.217	0.168	0.188	0.168
Suffolk	0.231	0.020	0.214	0.019	0.248	0.169	0.199	0.169
Wallaceton	0.230	0.021	0.225	0.021	0.190	0.142	0.146	0.142
West Point	0.272	0.022	0.248	0.021	0.234	0.177	0.234	0.177
Williamsburg	0.210	0.019	0.192	0.019	0.256	0.171	0.269	0.171
Hampton	0.336	0.220	0.312	0.021	0.185	0.170	0.188	0.169
Norfolk Airport	0.227	0.020	0.230	0.020	***0.140***	***0.176***	0.176	0.175
Norfolk	0.243	0.020	0.245	0.020	***0.152***	***0.180***	***0.171***	***0.180***
Oceana	0.255	0.021	0.255	0.021	0.186	0.180	0.200	0.179

List of Figures

FIGURE 1. The study area in the southeastern Virginia showing Global Historical Climatology Network-Daily (GHCN-D) stations.

FIGURE 2: Precipitation distribution at GHCN-D observation stations for 1950-2010 at nine locations of the study area.

FIGURE 3. Analysis of the daily maximum precipitation trends for 1950-2010 at nine GHCN-D locations of the study area. The blue line represents the average of the five high precipitation events. The red bar indicates the trend direction

FIGURE 4. Estimation of the precipitation ratio (high (> 90th percentile) to non-high) for 1950-2010 at nine GHCN-D locations of the study area. The bar represents the number of precipitation events greater than the 90th percentile.

FIGURE 5. Comparison of the maximum precipitation trends for 1950-2005 at nine GHCND locations of the study area among the daily CMIP5 MACA simulation, hourly Weather Forecasting and Research (WRF) model, and daily GHCND observation. The shaded region represents the uncertainty generated by the 15 CMIP5 MACA simulation models.

FIGURE 6. Future extreme precipitation analysis using the Theil-Sen estimation for 2016-2099 using RCP 4.5 and RCP 8.5 scenarios for the nine locations.

FIGURE 7. Spatial distribution of the annual extreme daily precipitation using two GCMs at southeastern Virginia. The red colour around few stations indicate higher extreme daily precipitation at respective GHCN-D stations.

FIGURE 8. Intensity-Duration-Frequency analysis for annual extreme daily precipitation using observed, GCMs-based historical, RCP 4.5 and RCP 8.5 scenarios at nine GHCN-D locations of the study area. The precipitation from observed and GCMs was analyzed from1950-2005, whereas the RCP 4.5 and 8.5 scenarios were analyzed from 2016-2099.

FIGURE 9. (a) Location map of the James River Basin. (b) Calibration (1991-2000) and Validation (2001-2009) of simulated (red) streamflow from Noah MP with Observed (green) USGS streamflow observations at the USGS_2042500 gauge station. (c) Calibration (1991-

2000) and Validation (2001-2009) of simulated (red) streamflow from Noah MP with Observed (green) USGS streamflow observations at the USGS_2042500 gauge station.

FIGURE 10. Annual average streamflow (ft3/s) (line plot) along with the annual precipitation (cm) (bar plot) for (a & b) Hampton (c & d) Suffolk (e & f) Williamsburg (g & h) Virginia Beach (I & j) at the USGS_02042500 streamflow gauge station. The red lines and bars indicate the BCC-CSM1.1 model, whereas blue lines and bars indicate CanESM2 model. The green lines and bars indicate the observed data regridded from NOAA stations.

FIGURE 11. A flood frequency curve for annual average flows for a) Hampton b) Suffolk c) Williamsburg d) Virginia Beach and e) the USGS_02042500 gauge station. The black and white lines refer to the mean streamflow of two models (BCC-CSMv1.1 and CanESM2) corresponding to the future period (2006-2097). The red circles indicate the simulated streamflow for the baseline period (1950-2016).
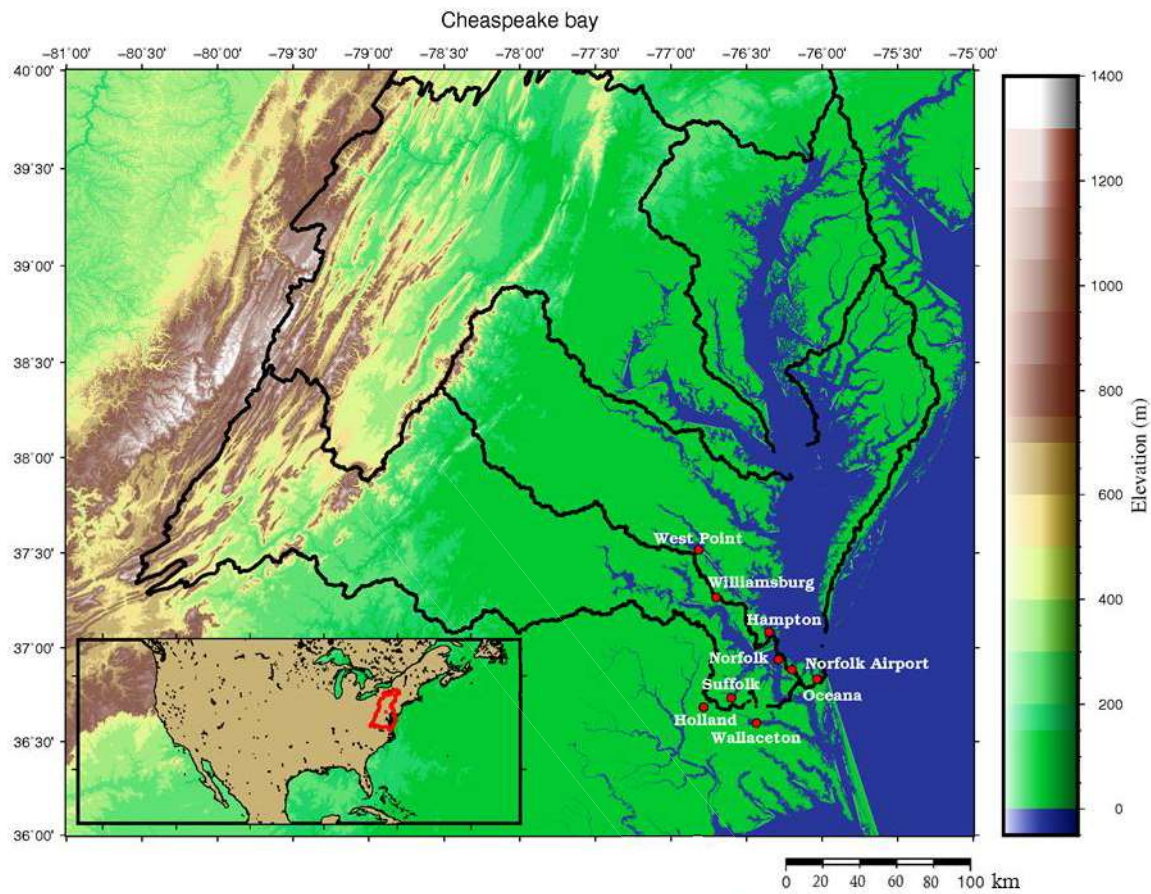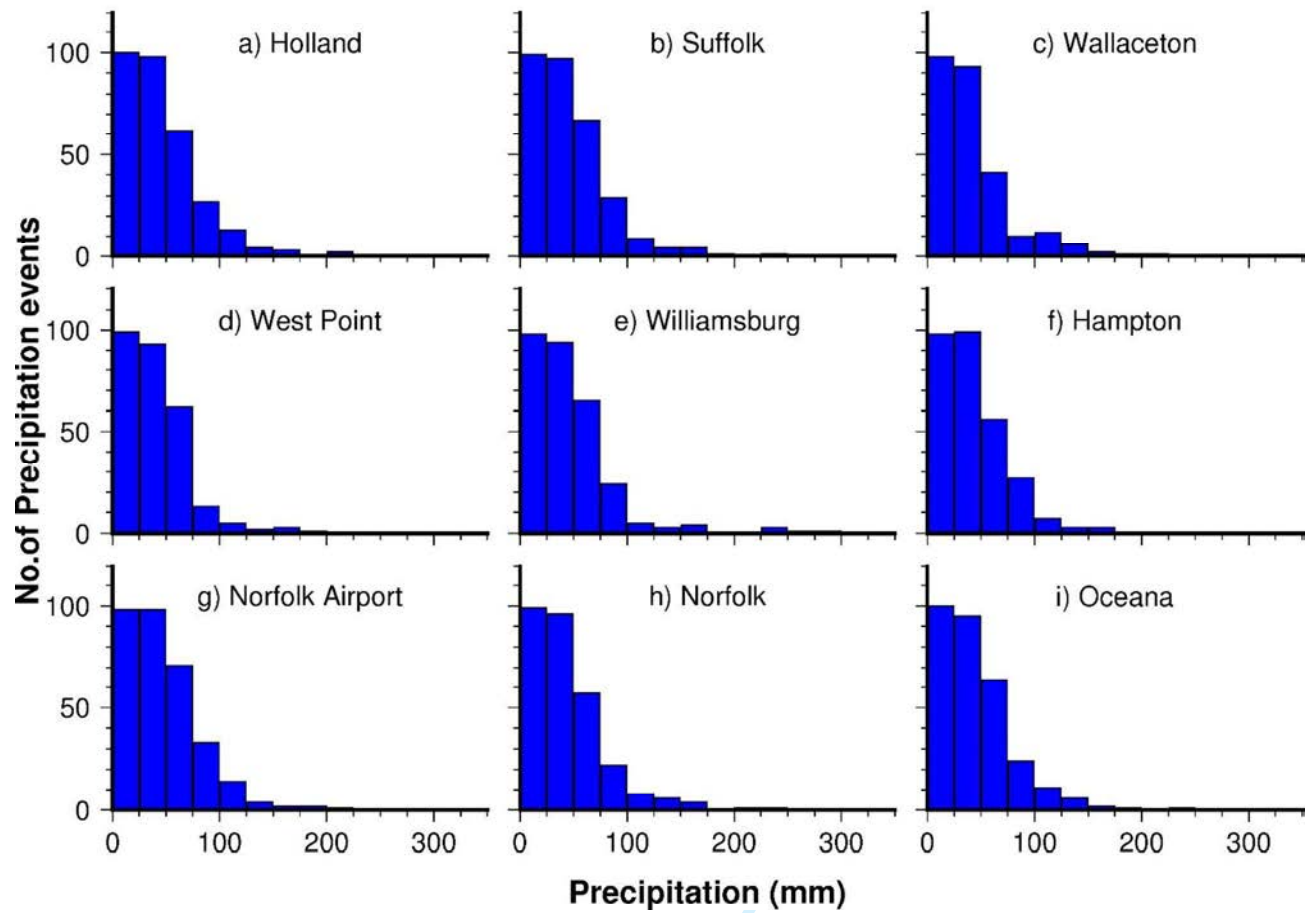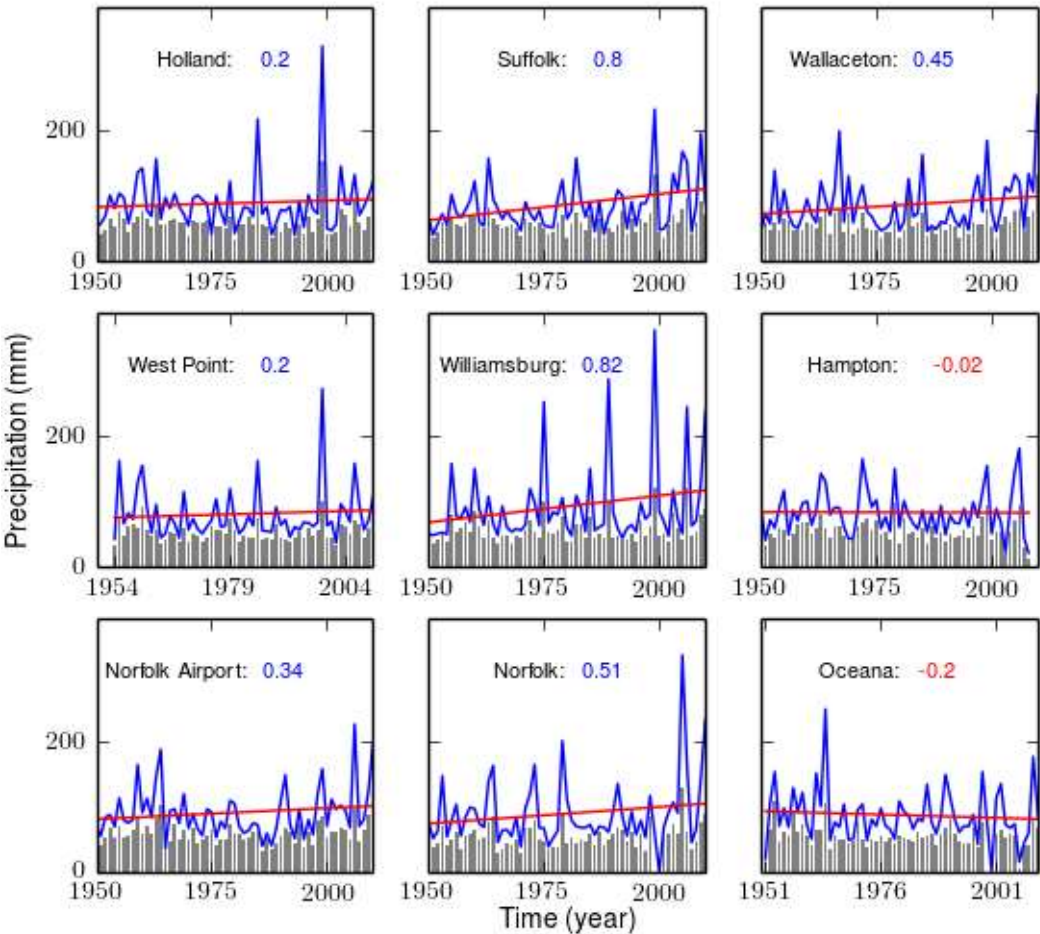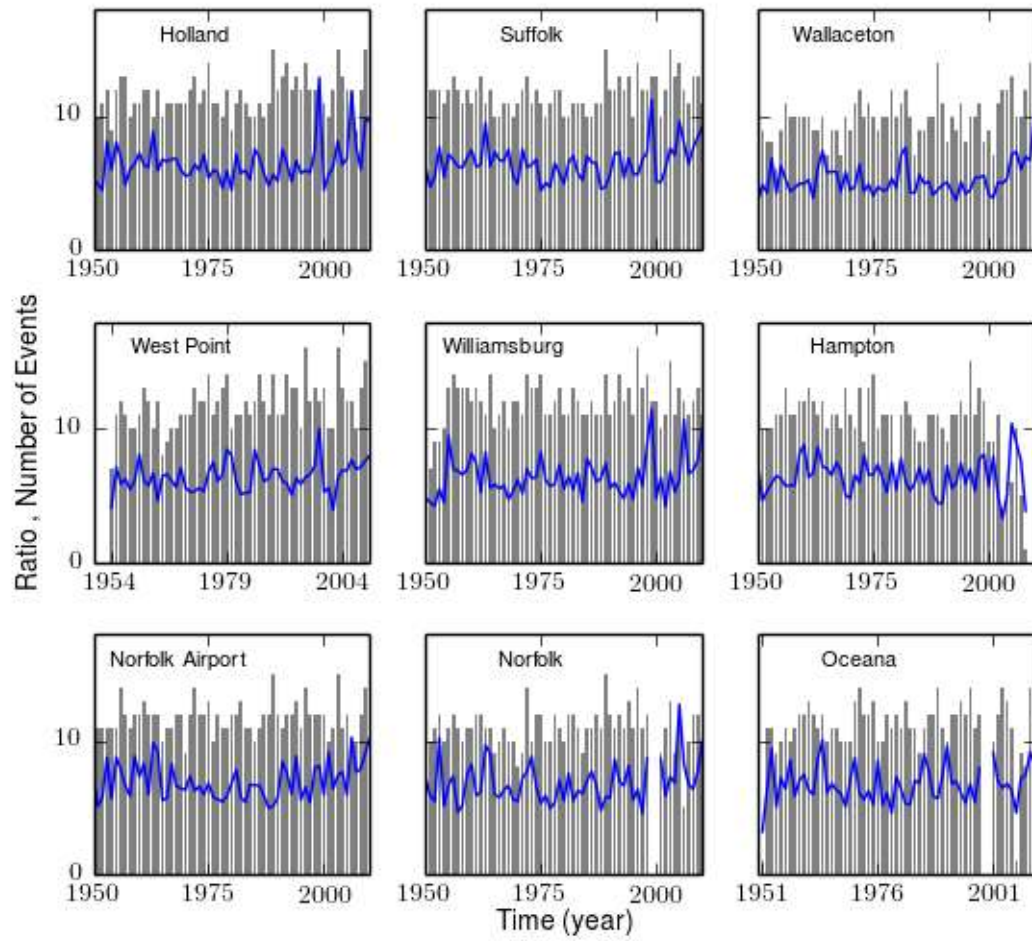
Figure 1

Figure 2

1
2
3
4
5
6
7
8
9
10
11
12
13
14
15
16
17
18
19
20
21
22
23
24
25
26
27
28
29
30
31
32
33
34
35
36
37
38
39
40
41
42
43
44
45
46
47
48
49
50
51
52
53
54
55
56
57
58
59
60

Figure 3

Figure 4

1
2
3
4
5
6
7
8
9
10
11
12
13
14
15
16
17
18
19
20
21
22
23
24
25
26
27
28
29
30
31
32
33
34
35
36
37
38
39
40
41
42
43
44
45
46
47
48
49
50
51
52
53
54
55
56
57
58
59
60

Figure 5

1
2
3
4
5
6
7
8
9
10
11
12
13
14
15
16
17
18
19
20
21
22
23
24
25
26
27
28
29
30
31
32
33
34
35
36
37
38
39
40
41
42
43
44
45
46
47
48
49
50
51
52
53
54
55
56
57
58
59
60

Figure 6

1
2
3
4
5
6
7
8
9
10
11
12
13
14
15
16
17
18
19
20
21
22
23
24
25
26
27
28
29
30
31
32
33
34
35
36
37
38
39
40
41
42
43
44
45
46
47
48
49
50
51
52
53
54
55
56
57
58
59
60

Figure 7

Figure 8

1
2
3
4
5
6
7
8
9
10
11
12
13
14
15
16
17
18
19
20
21
22
23
24
25
26
27
28
29
30
31
32
33
34
35
36
37
38
39
40
41
42
43
44
45
46
47
48
49
50
51
52
53
54
55
56
57
58
59
60

Figure 9

Figure 10

1
2
3
4
5
6
7
8
9
10
11
12
13
14
15
16
17
18
19
20
21
22
23
24
25
26
27
28
29
30
31
32
33
34
35
36
37
38
39
40
41
42
43
44
45
46
47
48
49
50
51
52
53
54
55
56
57
58
59
60

Figure 11